European Journal of Pharmacology 929 (2022) 175128

Contents lists available at ScienceDirect

European Journal of Pharmacology

journal homepage: www.elsevier.com/locate/ejphar

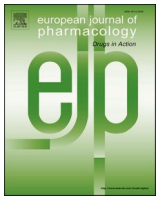

Novel purine analogues regulate IL-1β release via inhibition of JAK activity in human aortic smooth muscle cells

Geena V. Paramel [a], Madelene Lindkvist [a], Berhane A. Idosa [a], Laila Sharon Sebina [a], Caroline Kardeby [a,b], Theano Fotopoulou [c], Dimitra Pournara [c], Eftichia Kritsi [c], Eleni Ifanti [c], Maria Zervou [c], Maria Koufaki [c], Magnus Grenegård [a], Karin Fransén [a,*]

[a] Cardiovascular Research Centre, School of Medical Sciences, Örebro University, Örebro, Sweden
[b] Institute of Cardiovascular Sciences, College of Medical and Dental Sciences, University of Birmingham, Birmingham, West Midlands, United Kingdom
[c] Institute of Chemical Biology, National Hellenic Research Foundation, Athens, Greece

ARTICLE INFO

Keywords:
Purine analogue
Atherosclerosis
NLRP3 inflammasome
IL-1β
Inflammation
JAK inhibitor

ABSTRACT

Purine analogues bearing a nitrate ester motif were previously discovered as cardioprotective and anti-inflammatory agents, but the anti-inflammatory mechanism remains to be established. We therefore investigated the anti-inflammatory effect of two purine analogues, MK118 bearing a nitrate ester moiety and the methyl-substituted analogue MK196 in Aortic Smooth Muscle Cells (AoSMCs), with emphasis on IL-1β release. The AoSMCs were stimulated with LPS with or without purine analogue, followed by ELISA, Olink proteomics, Western blot and real time PCR of NLRP3 inflammasome components. Both purine analogues inhibited the release of proteins involved in inflammation, such as TRAIL, CCL4, CSF1 and IL-1β in AoSMCs, as well as intracellular gene and protein expression of IL-1β and NLRP3 inflammasome components. MK196, but not MK118, also inhibited the LPS-induced release of IL-7, CXCL10, PD-L1, FLT3L and CCL20. We also showed that MK118 and possibly MK196 act via inhibition of JAKs. *In silico* studies showed that the purine moiety is a competent hinge binding motif and that the purine-piperazine scaffold is well accommodated in the lipophilic groove of JAK1-3. Both compounds establish interactions with catalytic amino acids in the active site of JAK1-3 and the terminal nitrate ester of MK118 was revealed as a promising pharmacophore.

Our data suggest that MK118 and MK196 inhibit the release of proinflammatory proteins in AoSMCs, and targets JAK1-3 activation. Purine analogues also inhibit the expression of NLRP3 inflammasome genes and proteins and may in the future be evaluated for anti-inflammatory aspects on inflammatory diseases.

1. Introduction

Chronic inflammation is implicated in a large number of diseases, including cardiovascular disease (CVD). Atherosclerosis is one of the underlying factors for CVDs and elevated levels of proinflammatory cytokines and chemokines play key roles in all stages of atherosclerosis (Ramji and Davies, 2015). Pro-inflammatory cytokines are being expressed by endothelial cells and smooth muscle cells in the lesion and affects the cardiovascular system, such as via the induction of chemoattractant chemokines like MCP-1/CCL2, and platelet-derived growth factor, responsible for smooth muscle cell proliferation (Hansson, 2009; Moyer et al., 1991; Libby, 2017).

Previously, the CANTOS trial showed that canakinumab treatment targeting the IL-1 levels is beneficial for survivors of myocardial infarction (Ridker et al., 2017). Targeted therapy against inflammatory mechanisms in atherosclerosis, such as reduced IL-1β production and release, is therefore a successful strategy for limiting atherosclerosis and additional CVDs (Ridker et al., 2017). However, biological therapy is usually very costly, suggesting that small molecules targeting inflammatory pathways may be a more cost-effective approach. Piperazine-linked purine analogues bearing a nitrate ester motif were previously designed and evaluated *in vitro* and *in vivo* Koufaki et al. (2012); Maugé et al. (2014). The most active compound, MK118, was shown to reduce infarct size (compound no 16 in Koufaki et al., 2012). Purine analogues were also shown to reduce ATP induced IL-1β release in THP-1 cells (Maugé et al., 2014), although their biological mechanism of action in vascular cells remains unclear.

The maturation and release of IL-1β is a two-step mechanism

* Corresponding author. School of Medical Sciences, Örebro University, 701 82, Örebro, Sweden.
E-mail address: karin.h.franzen@oru.se (K. Fransén).

https://doi.org/10.1016/j.ejphar.2022.175128
Received 18 March 2022; Received in revised form 16 June 2022; Accepted 24 June 2022
Available online 2 July 2022

involving priming and activation of the NLRP3 inflammasome. Priming can occur via Pathogen-Associated Molecular Patterns (PAMPs), such as lipopolysaccharide (LPS), that are recognized by pattern-recognition receptors (PRRs; Martinon and Tschopp, 2005) and mediated by toll-like receptors (TLRs), TNFR and Myd88, which initiate transcription of pro-IL-1β and NLRP3 via NF-kB (Pellegrini et al., 2017). The second step assembles NLRP3, apoptosis-associated speck-like protein containing a CARD (ASC) and pro-caspase-1, which forms the NLRP3 inflammasome which induce maturation of pro- IL-1β into IL-1β that is ultimately released from the cell (Bauernfeind et al., 2011). It has also been shown that LPS can induce the JAK/STAT pathway and that IL-1β may be co-regulated by STAT3 (Samavati et al., 2009). Activation of JAKs lead to STAT phosphorylation, dimerization, nuclear translocation and DNA binding (Villarino et al., 2015). In addition, TLR4 ligands such as LPS, have been shown to phosphorylate STAT3 via Myd88 and TRIF in melanoma cells (Fu et al., 2020). However, the role of the JAK/STAT signaling pathway in aortic smooth muscle cells (AoSMCs) and its relation to NLRP3 inflammasome activation and IL-1β release in CVD remains to be further explored.

The aim of the present study was to elucidate the underlying molecular anti-inflammatory mechanism of two novel purine analogues, the nitrate ester bearing MK118 analogue and the methyl substituted MK196 derivative (Fig. 1) in vascular cells. The study investigated the role of MK118 and MK196 on the release of inflammatory proteins from AoSMCs, with specific emphasis on IL-1β release and NLRP3 inflammasome activation. Subsequent *in vitro* studies on the JAK/STAT pathway and *in silico* evaluation of their interactions in the catalytic site of JAKs were performed.

2. Materials and methods

2.1. Antibodies

NLRP3 (Cat. #MAB3724, 1:1000, Abnova, Taipei City, Taiwan), Anti-ASC/TMS1 (Cat. #3291-100, 1:500, BioVision, Milpitas, CA, USA), pro-IL-1β (Cat. #GTX100793, 1:1000, GeneTex, Hinschu City, Taiwan), GAPDH (Cat. #SC-25778, 1:1000, Santa Cruz Biotechnology, Dallas, TX, USA), STAT3 (Cat. #4904, 1:2000, Cell Signaling Technology, Dallas, MA, USA), Phosphorylated-STAT3 (Tyr705; Cat. #9131, 1:1000, Cell Signaling Technology).

2.2. Chemical synthesis of MKs

The synthesis and analytical data for MK118 (compound 16, 6-[4-(6-Nitroxyhexanoyl)piperazin-1-yl]-9H-purine) are reported in (Koufaki et al., 2012). The synthesis and the analytical data for MK196 (6-[4-Hexanoyl-(piperazin-1-yl)]-9H-purine) are included in Supplementary information S1 (Scheme A).

2.3. Cell culture

Human aortic smooth muscle cells (AoSMCs; Thermo Fisher Scientific, Waltham, MA, USA) were grown in Gibco™ Medium 231 including 10% Gibco™ smooth muscle growth supplement (SMGS) and Penicillin-Streptomycin (0.1U/mL Penicillin +100 ng/ml streptomycin, PEST antimicrobial; Gibco/Thermo Fisher Scientific) in 75 cm^2 culturing flasks at 37 °C with a 5% CO_2 atmosphere. Cells between passage 6–9 were used for the experiments.

2.4. Treatments of AoSMCs with MK118 and MK196

The AoSMCs were seeded at a concentration of 1.5×10^5 cells/well in six well plates. Cells were treated with 100 ng/ml LPS for 24 h in the presence or absence of increasing concentrations of MK118 or MK196 (Fig. 1), except for Western blot analyses of STAT signaling, where the treatment was 30 min.

Cell culture supernatants were collected and centrifuged at 5000×*g* for 10 min and stored at −80 °C for ELISA analysis. Cell lysates were stored at −80 °C and used for mRNA expression and Western blot analysis.

2.5. Cell viability and cytotoxicity assay

The viability of AoSMCs was determined using Neutral red uptake assay. In brief, cells were plated in 96-well plates at 5000 cells/well and cultured to 95% confluency. The cells were treated with 100 μM of MK118 or MK196 for 24 h s. Cells incubated in DMSO served as vehicle control. Cell viability was assessed by incubating the cells with 5 μg/ml neutral red (Sigma Aldrich/Merck, Cat. #N4638, Burlington, MA, USA) post treatment in the complete cell culture medium for 4 h. The medium was discarded, and the cells were rinsed with 1X PBS. The de-staining solution containing 100 μl of 1% acetic acid in 50% ethanol was added to wells to solubilize the neutral red dye and the absorbance was spectrophotometrically measured at 540 nm.

2.6. Olink Proseek Multiplex Assay

Culture medium from MK118 and MK196 treated AoSMCs from

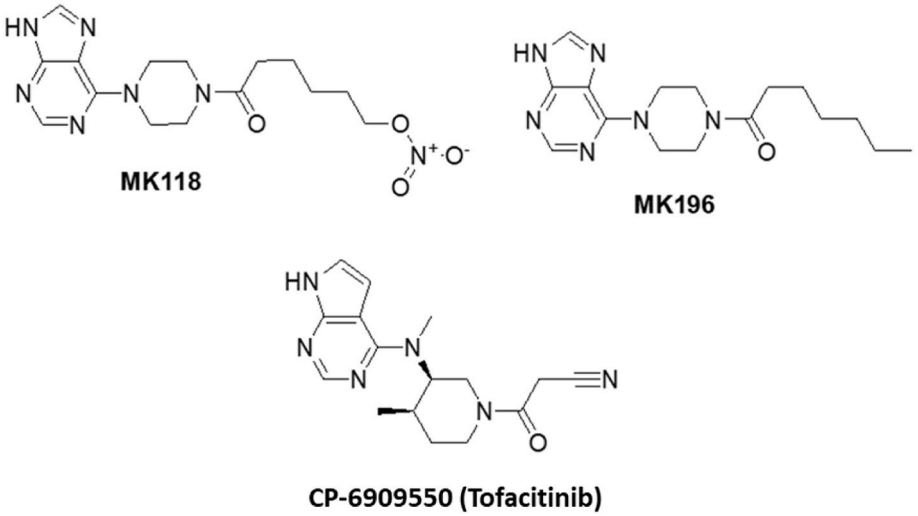

Fig. 1. Chemical structures of the purine analogues MK118 and MK196 the pan-JAK inhibitor CP-6909550 (Tofacitinib).

three individual experiments were analyzed utilizing the Inflammation panel from Olink Proteomics (Uppsala, Sweden). The panel contains an array of 92 established protein biomarkers for inflammation (https://www.olink.com/), utilizing the Olink Proseek Multiplex Assay using proximity extension assay (PEA) technology (Assarsson et al., 2014; Lundberg et al., 2011). The protein analysis is reported as normalized protein expression levels (NPX). The NPX values are Ct values normalized by the subtraction of values for extension control, and an interpolate control. Protein quantities were log2 transformed using Olink Wizard GenEx (MultiD Analyses, Gothenburg, Sweden). Additional information on assay validation and performance are available from the manufacturer's webpage (https://www.olink.com/products-services).

2.7. Western blot of protein extracts from AoSMCs

Extracted protein from cell lysates were quantified using the Pierce BCA Protein Assay Kit (Thermo Fisher Scientific). For inflammasome components, the protein lysates (10–15 μg) were separated using 4–20% Criterion™ TGX™ Precast Gels (Bio-Rad Laboratories, Hercules, CA, USA) and transferred onto nitrocellulose membranes (BioRad) using a Trans-Blot® Electrophoretic Transfer Cell (BioRad). Proteins were visualized using a reversible protein stain (Memcode/Thermo Fisher Scientific). For STAT-signalling, the protein lysates (20 μg) were separated using NuPAGE™ 5–12% Bis-Tris Gels (Thermo Fisher Scientific, Carlsbad, USA). Magic Mark™ XP and Novex® Sharp Pre-Stained protein standards (both from Thermo Fisher Scientific) were used to determine molecular weight. Proteins were blotted on Immobilion® FL Transfer Membrane (Merk Millipore Ltd. Cork, Ireland). All membranes were incubated overnight with primary antibodies diluted in 5% BSA-TBS-T and 0.02% sodium azide. Blots were visualized using advanced chemiluminescence BioRad ChemiDoc™ MP Imaging System (BioRad) or Li-Cor Odyssey Fc imager (LI-COR® Biosciences UK Ltd, Cambridge, UK). GAPDH was used as a loading control.

2.8. RNA extraction, cDNA preparation and quantitative real-time PCR (qRT-PCR)

Total RNA was extracted from AoSMCs using the E.Z.N.A total RNA kit (Omega Bio-Tek, Norcross, GA, USA) in accordance with the manufacturer's instructions. The cDNAs were prepared using High-Capacity cDNA Reverse Transcription Kit (Thermo Fisher Scientific) and analyzed for the expression of *IL1B* (Hs00174097), *NLRP3* (Hs00366465) and *CASP1* (Hs00354836) using TaqMan universal PCR master mix, TaqMan primers and probes using QuantStudio 7 Flex Real-Time PCR system (Thermo Fisher Scientific) according to the manufacturer's instructions. Data was normalized relative to *PPIB* (Hs00168719) as house-keeping gene.

2.9. Kinase activity assay

Select Screen Kinase Profiling Services were used to evaluate MK118 or MK196 as a JAK1-3 kinase inhibitor. These kinases were evaluated against increasing concentrations of MK118 or MK196 and ATP according to KM app standard protocol concentrations (JAK1: 87 μM; JAK2: 31 μM; JAK3: 14 μM). The Z'LYTE kinase analysis technology was used, which is based on fluorescence resonance energy transfer (FRET) technology and measures the lack of substrate phosphorylation upon kinase inhibition. More information about the Select Screen Kinase Profiling Services is available on the ThermoFisher Scientific website (https://www.thermofisher.com/se/en/home/products-and-services/services/custom-services/screening-and-profiling-services.html).

2.10. In silico studies to elucidate the interactions of MK118 and MK196 at the ATP binding site of JAK1-3

The examined structures were prepared at the optimum pH = 7.0 ± 0.5 (Schrödinger Release 2020-3, 2020a) and subjected to molecular docking studies performing the Standard (SP) and Extra (XP) Precision mode of Glide (Schrödinger Release 2020-3, 2020b). The crystal structures of JAK1 (PDB: 3EYG), JAK2 (PDB: 3FUP) and JAK3 (PDB: 3LXK) complexed with the known JAK inhibitor CP-690550 (Tofacitinib) were subjected to Protein Preparation (Schrödinger Release 2020-3, 2020c) and a grid box with dimensions 10 × 10 × 10 Å was generated. Missing residues and hydrogens were added, and restrained energy minimization followed using OPLS_2005 force field.

Molecular Dynamics Simulations (MD) of MK118:JAK1-3 and MK196:JAK1-3 docked complexes were carried out using the Desmond software (Schrödinger Release 2020-3, 2020d). For the examined systems setup, TIP4P was defined as the solvent model and the examined complexes were inserted in an orthorhombic box with volume 373512, 389244 and 348615 Å3, respectively. Also, OPLS_2005 force field was utilized and the systems were neutralized by adding 1 Cl^- ion for JAK1 complex, 6 Na^+ ions for JAK2 complex and 2 Na^+ ions for JAK3 complex. Subsequently, modelled systems were relaxed and then subjected to 100 ns MD simulations in the NPT ensemble class. During the simulation, the temperature was maintained at 300 K using the Nose-Hoover chain thermostat method with a 1.0 ps relaxation time and the pressure was maintained at 1 bar using Martyna-Tobias-Klein barostat method.

2.11. Statistical analysis

GraphPad Prism was used to perform the statistical analysis (GraphPad Prism 9 software). One-way ANOVA with Sidak's correction (Olink data) or Bonferroni multiple correction was used to analyze the differences between the experimental groups. The IC50 values were calculated by nonlinear regression of inhibitor concentration versus response in GraphPad Prism. All data are represented as mean ± standard error of the mean (SEM). Differences associated with P values $\leq$ 0.05 were considered statistically significant.

3. Results

3.1. The purine analogues MK118 and MK196 inhibit IL-1β release from AoSMCs

In order to study the role of purine analogues on LPS-induced vascular inflammatory response in AoSMCs, we evaluated the role of MK118 and MK196 on IL-1β release with ELISA. Stimulation with 100 ng/ml LPS resulted in a significant increase of IL-1β release after 24 h (MK118: N = 3; p = 0.049; MK196: N = 3; p = 0.014). As shown in Figure 2A100 μM of the purine analogue MK118 or MK196 reduced LPS induced IL-1β release (MK118: N = 3; p = 0.032; MK196: N = 3; p = 0.0065; Fig. 2A). Therefore, we used the concentration of 100 μM MK118 and MK196 for the subsequent experiments.

Cell viability was evaluated using a Neutral red drug-cytotoxicity assay, which detects lysosomal activity and membrane permeability in viable cells. We investigated the viability of AoSMCs after treatment with 100 μM MK118 or MK196 for 24 h. The cell viability was not affected by MK118 or MK196 (MK118: N = 3; $p > 0.05$; MK196: $N = 3$; $p > 0.05$; Fig. 2B), suggesting that the decrease in IL-1β release could not be explained by reduced cell viability at the given concentration.

3.2. The purine analogues MK118 and MK196 affect the release of several inflammatory proteins from AoSMCs

Except for the ability of MK118 and MK196 to reduce the LPS induced IL-1β release in AoSMCs, additional pathways and molecular targets are unknown. Therefore, we performed proteomics screening

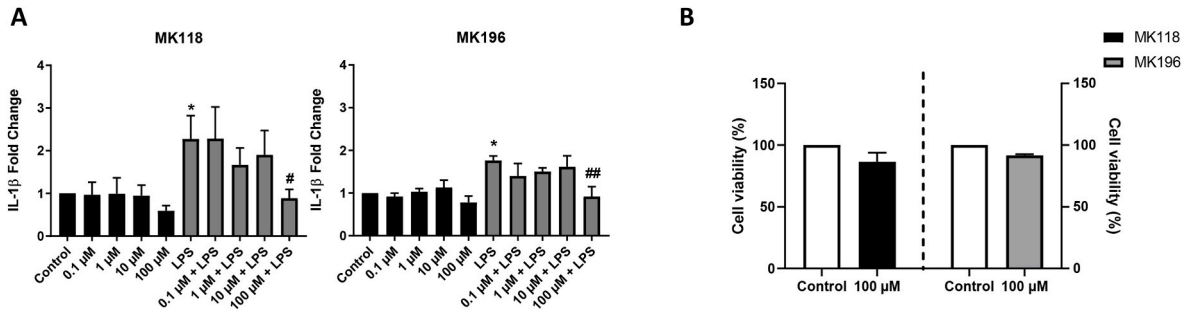

Fig. 2. Effect of the purine analogues MK118 and MK196 on cell viability and IL-1β release of AoSMCs. A. ELISA of IL-1β release (MK118: Control, 25.84 ± 4.66 pg/ml; LPS, 60 ± 10.97 pg/ml; 100 μM MK118 + LPS, 21.52 ± 4.50 pg/ml; MK119: Control, 56.21 ± 8.68 pg/ml; LPS, 98.85 ± 15 pg/ml; 100 μM MK118 + LPS, 55.46 ± 22.19 pg/ml) after 24 h treatment of purine analogues and 100 ng/ml LPS (MK118: *p = 0.049, $^{\#}$p = 0.032, MK196: *p = 0.014, $^{\#\#}$p = 0.0065). Results of $n = 3$ are displayed as mean± SEM. One-way ANOVA * = compared to control, # = compared to LPS. **B.** Neutral Red uptake assay after 24 h treatment (p > 0.05).

using Olink Proseek Multiplex Assay/Inflammation panel and assessed the inflammatory proteins released in the medium after treatment with LPS and purine analogue. In total, 48 proteins out of 92 were detected in the cell medium using the Inflammation panel (Supplementary information S2). In the inflammation panel, 92 different proteins were investigated and of which the LPS induced expression of TRAIL, CCL4 and CSF1 were significantly downregulated by both MK118 and MK196. In addition, the LPS induced expression of CCL3 was significantly downregulated by MK118 and a similar trend of reduction was observed after MK196 treatment (Fig. 3A–D; $p = 0.077$).

The LPS induced expression of the five proteins, IL-7, CXCL10, PD-L1, FLT3L and CCL20, were solely downregulated by MK196 (Fig. 4A, D, F, G and H). Although we could not observe any significant upregulation by LPS for LAP TGF-beta-1, AXIN or FGF-5 (Fig. 4B and C and Fig. 3E), we found a significant reduction of release of these proteins after treatment with MK196. No additional proteins were significantly

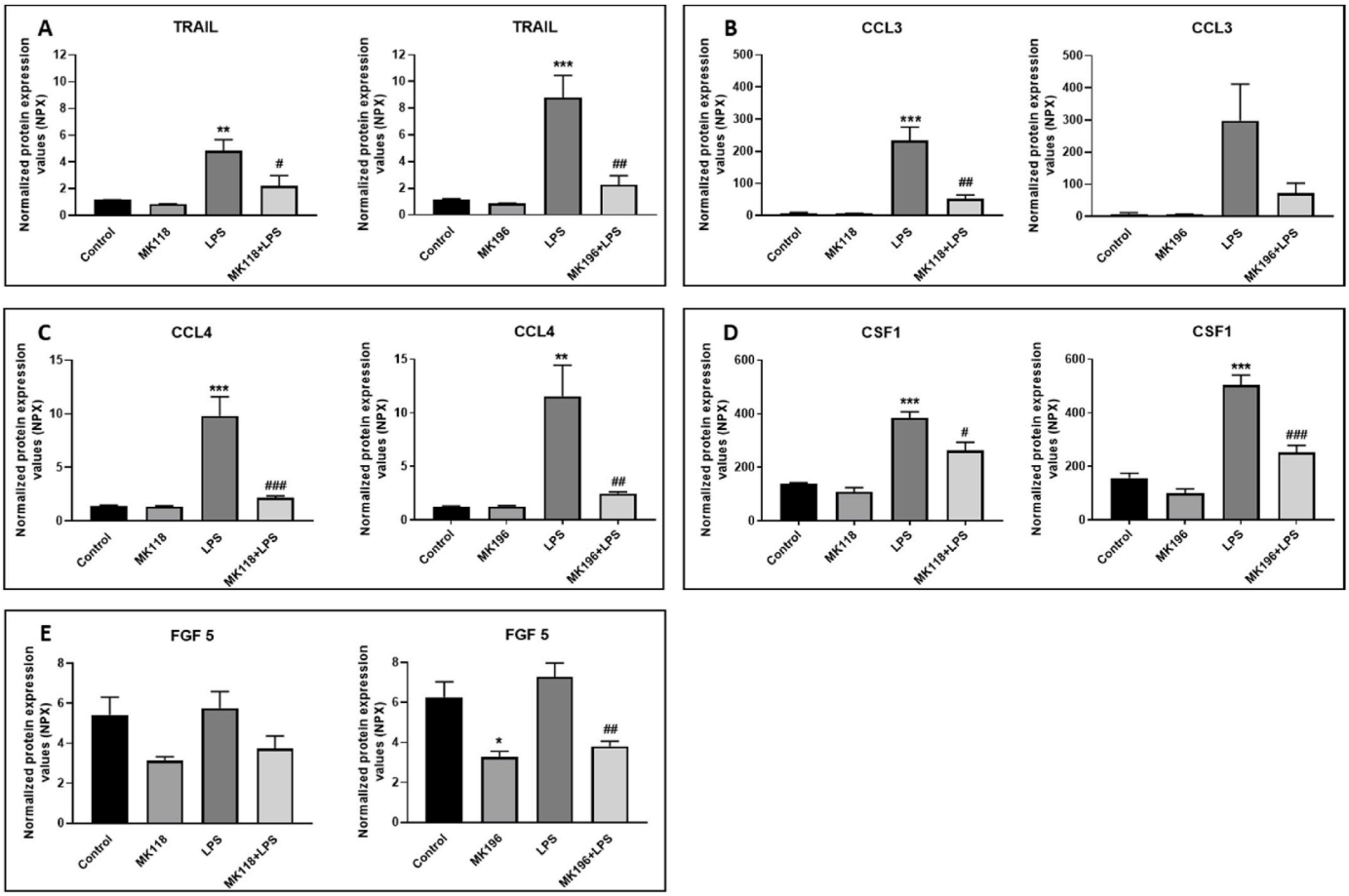

Fig. 3. Protein release of AoSMCs regulated by both MK118 and MK196. Treatment for 24 h by MK196 (100 μM) and LPS (100 ng/ml) before cell culture medium was collected and analyzed by the Olink Inflammation Panel. Differently regulated proteins by both MK118 and MK196 were **A.** TRAIL (MK118 $^{**}p = 0.0049$, $^{\#}p = 0.0318$, MK196 $^{***}p = 0.0009$, $^{\#\#}p = 0.0026$). **B.** CCL3 (MK118 $^{***}p = 0.0002$ $^{\#\#}p = 0.0011$). **C.** CCL4 (MK118 $^{***}p = 0.0005$ $^{\#\#\#}p = 0.0009$, MK196 $^{**}p = 0.0032$, $^{\#\#}p = 0.0069$). **D.** CSF1 (MK118 $^{***}p = 0.0001$, $^{\#}p = 0.0105$, MK196 $^{***}p < 0.0001$ $^{\#\#\#}p = 0.0004$). **E.** FGF 5 (MK196 $^{*}p = 0.0157$, $^{\#\#}p = 0.0067$, MK196 $^{***}p < 0.0001$ $^{\#\#\#}p = 0.0004$). Results of $n = 3$ are displayed as mean± SEM. One-way ANOVA * = compared to control, # = compared to LPS.

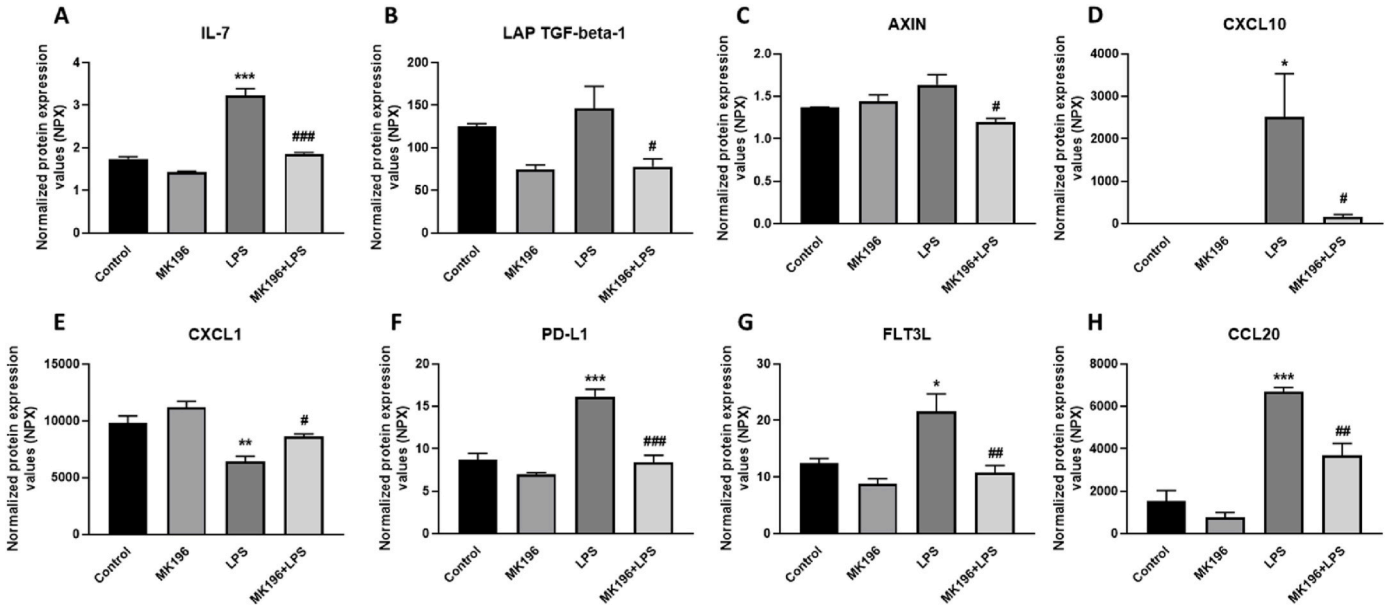

Fig. 4. MK196-regulated protein release of AoSMCs. Treatment for 24 h by MK196 (100 μM) and LPS (100 ng/ml) before cell culture medium was collected and analyzed by the Olink Inflammation Panel. Differently regulated proteins were **A.** IL-7 (***$p < 0.0001$, $^{\#\#\#}p < 0.0001$). **B.** LAP TGF-beta-1 ($^{\#}p = 0.0279$). **C.** AXIN ($^{\#}p = 0.0105$). **D.** CXCL10 (*$p = 0.0270$, $^{\#}p = 0.0369$). **E.** CXCL1 (**$p = 0.0028$, $^{\#}p = 0.0303$). **F.** PD-L1 (***$p = 0.0002$, $^{\#\#\#}p = 0.0002$). **G.** FLT3L (*$p = 0.0187$, $^{\#\#}p = 0.0070$). **H.** CCL20 (***$p < 0.0001$, $^{\#\#}p < 0.0027$). Results of $n = 3$ are displayed as mean± SEM. One-way ANOVA * = compared to control, $^{\#}$ = compared to LPS.

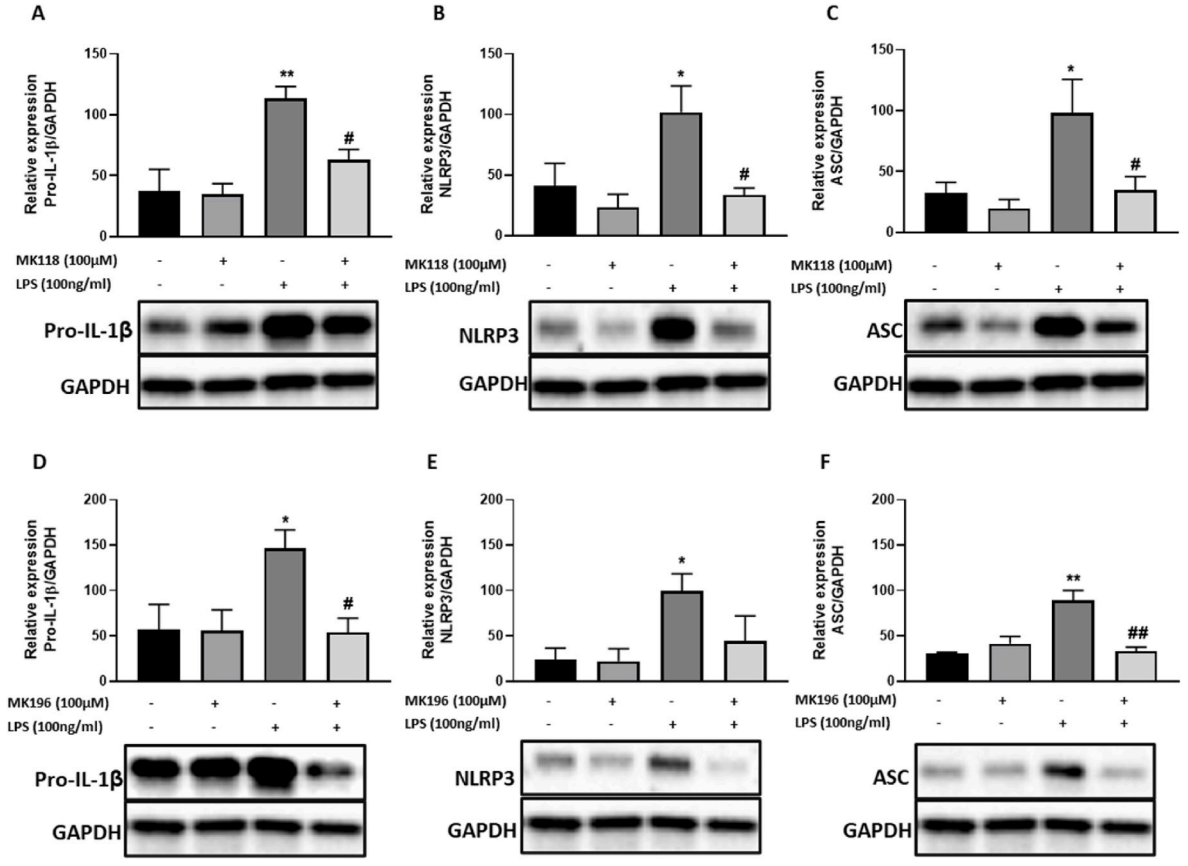

Fig. 5. Protein expression of NLRP3 inflammasome components in AoSMCs treated with 100 μM of the purine analogues MK118 and MK196 with or without 100 ng/ml LPS. Treatment for 24 h by MK118 **(A–C)** or MK196 **(D–F)** followed by Western blot of **A.** pro-IL-1β (**$p = 0.0054$, $^{\#}p = 0.047$). **B.** NLRP3 (*$p = 0.048$, $^{\#}p = 0.028$). **C.** ASC (*$p = 0.040$, $^{\#}p = 0.047$). **D.** pro-IL-1β (*$p = 0.043$, $^{\#}p = 0.037$). **E.** NLRP3 (*$p = 0.049$, $^{\#}p = 0.16$). **F.** ASC (**$p = 0.0013$, $^{\#\#}p = 0.0017$). Results of $n = 3$ are displayed as mean± SEM. One-way ANOVA * = compared to control, $^{\#}$ = compared to LPS.

regulated by only MK118.

3.3. Protein and gene expression of the NLRP3 inflammasome components in AoSMCs

We further investigated the effect of the purine analogues MK118 and MK196 on the LPS-induced intracellular mRNA and protein expression levels of the NLRP3 inflammasome components. Western blot was performed on cell lysates for pro-IL-1β, NLRP3 and ASC, from AoSMCs treated with LPS in the presence and absence of MK118 or MK196. The intracellular LPS-induced protein expression of pro-IL-1β, NLRP3 and ASC in AoSMCs was significantly reduced upon treatment with MK118 (N = 3; pro-IL-1β, 37 kDa, p = 0.047; NLRP3, p = 0.028; ASC, $p = 0.047$; Fig. 5A–C). In a similar fashion, there was a significant reduction of the intracellular protein expression of pro-IL-1β, and ASC, but not NLRP3, after MK196 treatment ($N = 3$; pro-IL-1β, 37 kDa, $p = 0.037$; NLRP3, $p = 0.16$; ASC, $p = 0.0017$; Fig. 5D–F).

The ability of MK118 and MK196 to reduce LPS-induced intracellular gene expression of *pro-IL-1B* was confirmed on mRNA level ($N = 3$; $p = 0.034$ and $p = 0.034$ respectively; Fig. 6A and E). The purine analogue MK118 was also able to reduce the transcriptional levels of *NLRP3* and *CASP1* (N = 3; p = 0.026 and p = 0.0059 respectively, Fig. 6B and D).

After MK196 treatment, a trend for reduced gene expression of *NLRP3* ($p = 0.078$) or *CASP1* ($p = 0.052$) was observed (Fig. 6F and H). The mRNA expression of ASC/*PYCARD* remained unaltered in response to LPS after treatment with MK118 or MK196 (Fig. 6C and G).

3.4. MK118 and MK196 inhibit JAKs

To further investigate the contribution of upstream targets to the observed inhibitory effects of MK118 and MK196, we evaluated the kinase activity of JAK1-3 in the presence of increasing concentrations of MK118 and MK196 via Select Screen™ Kinase Profiling Services by Thermo Fisher Scientific. Our results show that MK118 and MK196 inhibited JAK isoenzymes in a concentration-dependent manner (Fig. 7A). Among the JAKs, JAK3 was slightly more potently inhibited (IC50 = 3.9 μM for MK118 and 5.7 μM for MK196), followed by JAK2 (IC50 = 5.5 μM for MK118 and 6.5 μM for MK196) and JAK1 (IC50 = 6.2 μM for MK118 and 8.0 μM for MK196).

To biologically verify the role of MK118 and MK196 as putative inhibitors of JAK1-3, we therefore analyzed STAT3 phosphorylation in the presence or absence of MK118 and MK196. Structures of MK118, MK196 and the commercial JAK inhibitor CP-690550 are displayed in Fig. 1. The purine analogue MK118 significantly inhibited the Tyr^{705} phosphorylation of STAT3 in AoSMCs after 30 min ($N = 3$; LPS vs MK118 + LPS, $p = 0.017$; Fig. 7B). The purine analogue MK196 did not significantly inhibit the STAT3 phosphorylation, although a trend of reduced STAT3 phosphorylation could be observed ($N = 3$, $p = 0.10$; Fig. 7B).

3.5. In silico studies to elucidate the interactions of MK118 and MK196 at the ATP-binding site of JAK1-3

The MD results for MK118 and MK196 revealed that the purine moiety is well accommodated in the active site of JAK1-3 preserving the crucial interactions with the hinge region through the whole simulation time. (Figs. 8–10). Details of the MD trajectories are provided in the Supplementary Figures S4-S7. The bound poses of Tofacitinib at JAK1-3 as retained from the respective crystal structures are presented in (Supplementary Figure S3) for comparison.

MK118 and MK196 at JAK1: A lipophilic pocket of JAK1 consisting of Ala906, Met956, Phe958, Leu1010 harbors the purine-piperazine scaffold reminiscent of the location of the pyrollo-pyrimidine feature of Tofacitinib. (Supplementary Figure S3) Both analogues contact the crucial hinge region amino acids Glu957 and Leu959 through H-bonding throughout the whole simulation time. (Fig. 8A and B).

Despite the flexibility of the alkyl chain, MK118 uses the nitro group to develop stable ionic interactions with the catalytic residues Asp1021 (DFG motif) and Lys908 (in the neighboring of the Gly loop) during the last 40 ns of the MD run (Fig. 8A). This conformation of the terminal nitro moiety pointing towards the Gly loop of the N-lobe mimics the orientation of the tofacitinib nitrile (Williams et al., 2009). Moreover, the carbonyl moiety by interacting via water mediated H-bonds with Ser963 (interface of the hinge region and aD-helix of the C-lobe) stabilizes further this orientation.

MK196 which is devoid of the terminal nitro moiety displays a more prominent flexibility of the alkyl chain in the active site. Interestingly though, the carbonyl moiety adopts an opposite orientation as compared with MK118 in order to enable direct and indirect H-bond interactions with the Gly loop (Glu883) and water mediated interactions with Asp1021 (DFG motif). The N atom at position −7 of the purine moiety is able to interact through a dense water network with the crucial Asp1021 (DFG), further contributing to the stabilization of the purine interactions

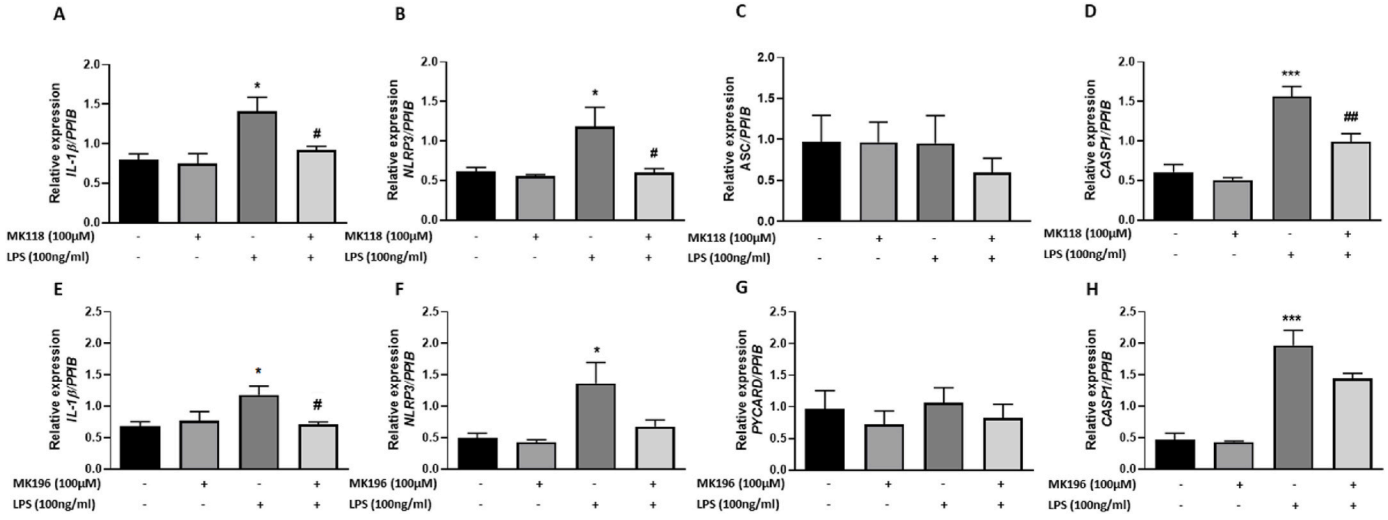

Fig. 6. Gene expression of NLRP3 inflammasome components in AoSMCs treated with 100 μM of the purine analogues MK118 and MK196 with or without 100 ng/ml LPS. Treatment for 24 h by MK118 **(A–D)** or MK196 **(E–G)** followed by quantitative real-time PCR analysis of **A.** *IL-1β* ($^{*}p = 0.011$, $^{\#}p = 0.034$), **B.** *NLRP3* ($^{*}p = 0.030$, $^{\#}p = 0.026$), **C.** *ASC* ($p > 0.05$), **D.** *CASP1* ($^{***}p = 0.0002$, $^{\#\#}p = 0.0059$), **E.** *IL-1β* ($^{*}p = 0.025$, $^{\#}$p = 0,034), **F.** *NLRP3* ($^{*}p = 0.018$), **G.** *ASC* ($p > 0.05$), **H.** *CASP1* ($^{\#\#}p = 0.0059$). Results of $n = 3$ are displayed as mean± SEM. One-way ANOVA * = compared to control, $^{\#}$ = compared to LPS.

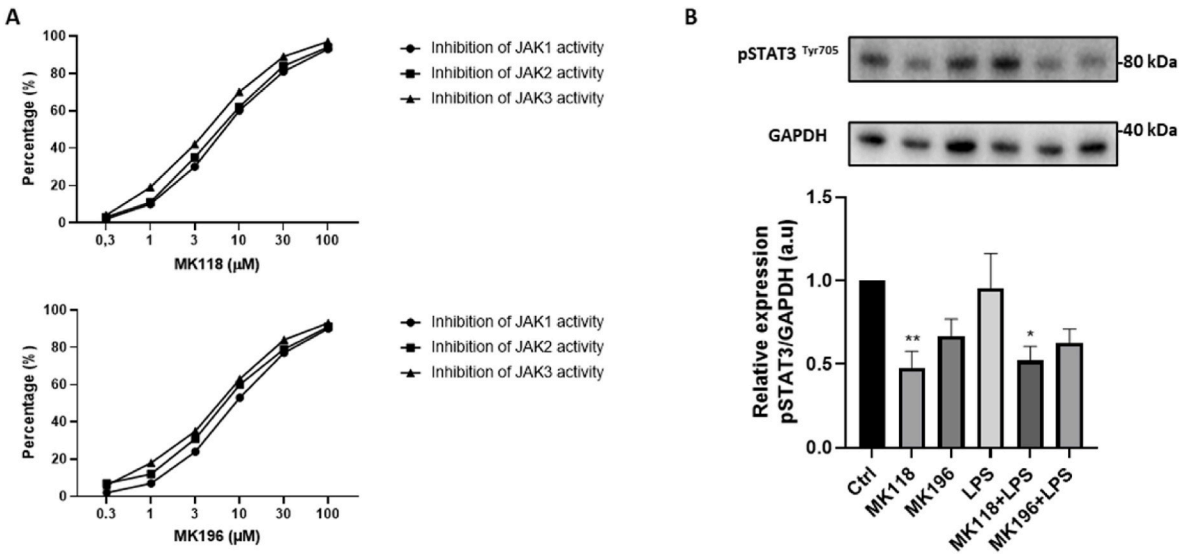

Fig. 7. JAK-inhibition by the purine analogues MK118 and MK196. A. Kinase activity evaluated via Select Screen Kinase Profiling Services. Performed in duplicates and shown as mean value. **B.** Western blot of phosphorylated STAT3 at Tyr^{705} in AoSMCs after 30 min treatment of 100 μM MK118, 100 μM MK196, 100 ng/ml LPS. Normalized to GAPDH ($*p = 0.017$, $**p = 0.0071$, $***p < 0.0001$). Results of $n = 3$ are displayed as mean± SEM. One-way ANOVA * = compared to control.

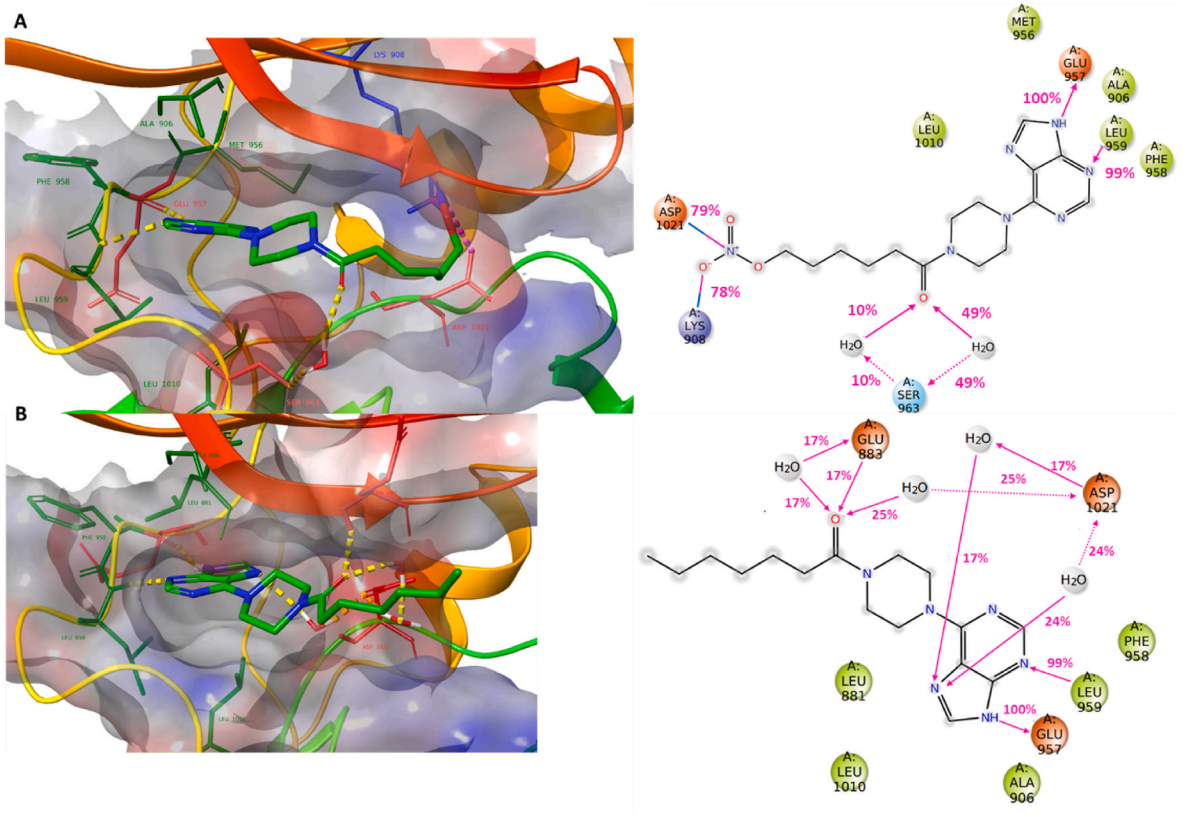

Fig. 8. (Left) Representative binding modes obtained from the MD simulation at JAK1 (pdb:3EYG) of (A) MK118 and (B) MK196. (Right) 2D ligand interaction diagrams of MK118 (60–100 ns) and MK196 (30–100 ns) indicating the frequency of occurrence of interactions. Figure made with Desmond software and Maestro interface.

with the hinge region. (Fig. 8B).

MK118 and MK196 at JAK2: The purine-piperazine feature of MK118 and MK196 is also well accommodated in the active site of JAK2 and the crucial interactions with the hinge region (Glu930 and Leu932) are conserved through the whole simulation time.

In this case, the lipophilic groove, which harbors the purine-piperazine scaffold consists of the aromatic ring of Tyr931, Leu983 (conserved amino acid corresponding to Leu1010 at JAK1), Ala880 (conserved amino acid corresponding to Ala906 at JAK1). This groove is considered critical for the stabilization of the binding within the active

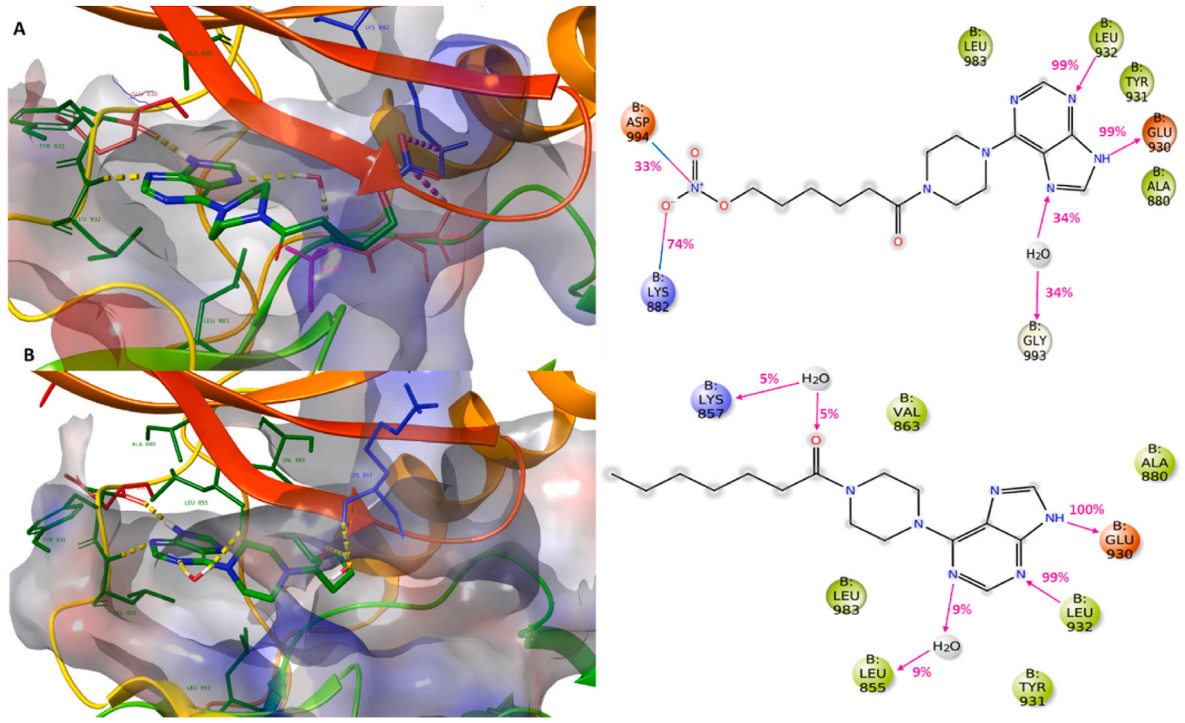

Fig. 9. (Left) Representative binding modes obtained from the MD simulation at JAK2 (pdb: 3FUP) of (A) MK118 and (B) MK196. (Right) 2D ligand interaction diagrams of MK118 (0–100 ns) and MK196 (70–100 ns) indicating the frequency of occurrence of interactions. Figure made with Desmond software and Maestro interface.

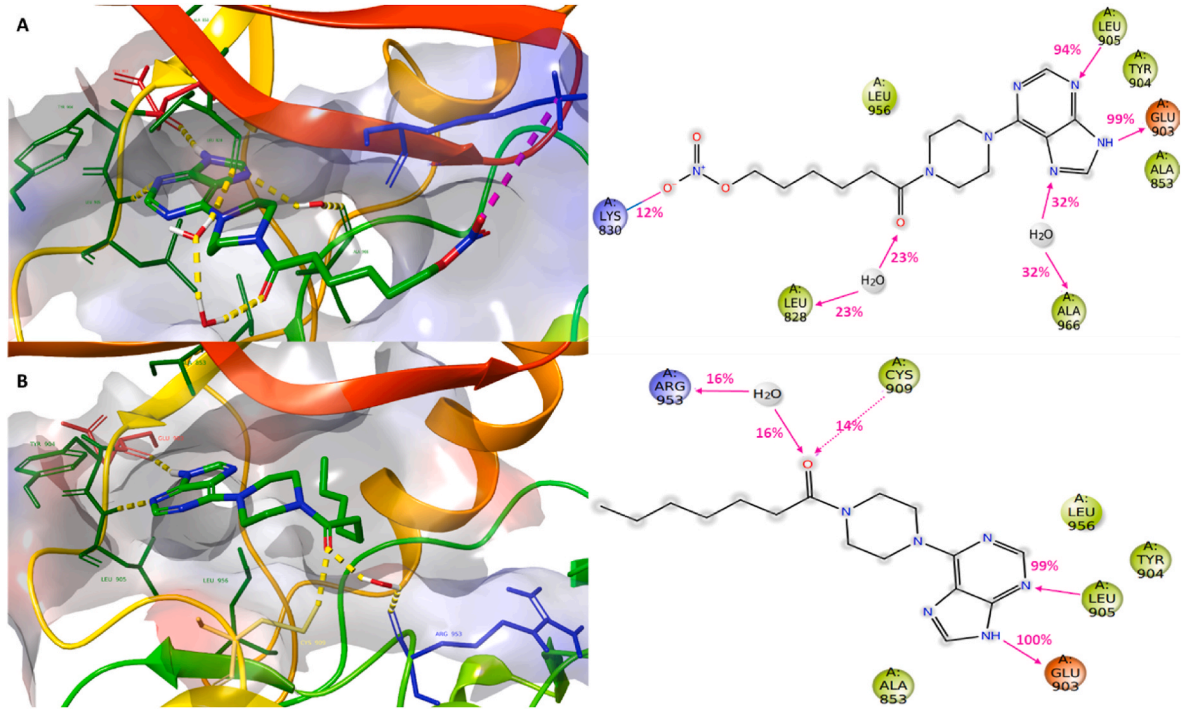

Fig. 10. (Left) Representative binding modes obtained from the MD simulation at JAK3 (pdb: 3LXK) of (A) MK118 and (B) MK196. (Right) 2D ligand interaction diagrams of MK118 (40–100 ns) and MK196 (40–100 ns) indicating the frequency of occurrence of interactions. Figure made with Desmond software and Maestro interface.

site of JAK2 (Lin et al., 2018).

The flexibility of the alkyl chain of MK118 is less pronounced as compared with JAK1, enabling the development of ionic interactions of the terminal NO with Lys882 (conserved amino acid corresponding to Lys908 at JAK1) for a significant period of the whole simulation time and to a lesser degree with Asp994 of the DFG motif (corresponding to Asp1021 at JAK1). Interaction with the described amino acids is considered critical for JAK2 binding (Lin et al., 2018, Fig. 9A).

Regarding MK196, the tight binding of the purine scaffold may also be supported by a water mediated H-bonding of the N atom at position-3 with Leu855 (located in β1 sheet preceding the Gly loop). In analogy with JAK1 results, the absence of the terminal nitro moiety is related to a more increased flexibility of MK196's alkyl chain. During the last 30 ns of the MD run, the compound adopts a conformation similar to that of MK118 enabling a water mediated interaction of the carbonyl moiety with the Gly loop (Lys857) for a limited time, an interaction that may influence the loop's flexibility (Vazquez et al., 2018, Fig. 9B).

MK118 and MK196 at JAK3: The hinge binding motif is also preserved against JAK3 where both MK118 and MK196 retain the conserved interactions with Glu903 and Leu905 during the whole simulation time. The hydrophobic groove which shelters the purine-piperazine scaffold consists of the amino acids Tyr904 and the conserved Ala853 and Leu956.

MK118 may also exploit the nitrogen atom at position-7 of purine to interact via water with the non-conserved Ala966 which precedes the DFG motif. The MK118 terminal nitrate ester is oriented towards the Gly loop where it stabilizes an ionic interaction with Lys830 although present for a limited period of time. MK118 uses its CO linker to form a water-mediated H-bonding with the conserved Leu828 (β1 sheet preceding the Gly loop, Fig. 10A).

As already described for JAK1 and JAK2, MK196 is associated with an increased mobility of the alkyl chain. Interestingly though, after 40 ns, the carbonyl moiety directly interacts with Cys909 which is unique for the JAK3 isoform. This residue has been recently exploited for the design of JAK3 specific inhibitors through covalent bonding (Thorarensen et al., 2017). Moreover, an indirect interaction is favored between CO with the conserved Arg953 located in the catalytic loop (Fig. 10B).

4. Discussion

Targeting IL-1β and its actions has been implicated as a novel era of anti-inflammatory therapy of CVDs (Libby, 2017). A novel group of small molecules with cardioprotective abilities are 6-piperazinyl-purine analogues which have been shown to reduce the infarct size in rabbit model (Koufaki et al., 2012). However, their anti-inflammatory role in vascular cells is still not known. Previously, we showed that the expression of several of the NLRP3 inflammasome components, such as *NLRP3*, *ASC*, *IL-1β* and *caspase-1* was elevated in atherosclerotic lesions (Parmel Varghese et al., 2016). In the present study, we showed that the two purine analogues MK118 and MK196, with or without a nitrate ester moiety respectively, were well tolerated at the given concentration and reduce the LPS-induced expression and release of IL-1β in AoSMCs. The LPS-induced expression of several of the additional NLRP3 inflammasome associated genes and proteins were altered. The LPS induced *NLRP3* mRNA and protein expression after treatment with MK118 was significantly reduced and a trend of reduction in expression of *NLRP3* mRNA and protein after MK196 treatment was observed. Taken together, this indicate that MK118 and possibly also MK196 affect signal 1 of NLRP3 inflammasome activation via abrogation of pro-IL-1β and NLRP3 transcription in AoSMCs. In addition, the LPS-induced protein expression of ASC was significantly reduced after MK118 or MK196 treatment, but could not be verified on the transcriptional level. Although ASC/*PYCARD* is mainly constitutively expressed, down-regulation of ASC/*PYCARD* has been described in cancer cells, due to methylation of promoter CpG island (Cornut et al., 2020), but the precise mechanism for ASC downregulation in vascular cells is unclear. We also observed a significantly reduced intracellular *CASP1* mRNA expression after MK118 and a trend of reduced *CASP1* mRNA expression after MK196 treatment. We were however unable to detect the active extracellular p20 component of caspase-1 in supernatants of AoSMCs via flow cytometry (data not shown). However, others have also found it challenging to study signal 2 of NLRP3 inflammasome activation in AoSMCs (Dautova et al., 2018) and the precise mechanism for the reduced IL-1β release remains elusive and an alternative explanation to the reduced IL-1β release may be possible.

To further explore the specific mechanism of MK118 and MK196 for IL-1β release, we therefore studied the involvement of JAK1-3 via STAT3 Tyr^{705} phosphorylation. Phosphorylation of STAT3 at the JAK specific phosphorylation site Tyr^{705}, is necessary for STAT dimerization, translocation to the nucleus and DNA binding (Samavati et al., 2009; Lai and Johnson, 2010; Schuringa et al., 2000). Moreover, TLR4 ligands, like LPS, have been associated with STAT3 mediated IL-1β release in several mouse and human cell types (Samavati et al., 2009; Fu et al., 2020; Sodhi et al., 2007; Lee et al., 2006). In the present paper, Thermo Fisher Select Screen Kinase Profiling Services showed that MK118 and MK196 (IC50 values around 5 μM) inhibit JAK1-3 in a concentration-dependent manner. In smooth muscle cells, we confirmed via Western blot that mainly MK118, inhibits basal STAT3 phosphorylation. Our data is also supported by previous studies, where other JAK inhibitors like stattic and AG490 inhibits IL-1β release (Samavati et al., 2009).

The differences between MK118 and MK196 are however small out of a pharmacological perspective, suggesting that the drugs are almost equipotent both in terms of targeting JAK1-3 and expression of NLRP3 inflammasome components. The commercial JAK inhibitor CP-6909550, was previously shown to reduce IL-1β release in GM-CSF induced neutrophils via the NLRP3 inflammasome (Furuya et al., 2018). Although MK118 and MK196 are almost equipotent, the purine analogue MK118 seems to be slightly more effective than MK196. However, we cannot exclude that the IL-1β reducing effect of MK118 and MK196 is due to inhibition of other kinases or alternative mechanisms. We previously showed that another purine analogue, MK128 (compound 15 in Koufaki et al., 2012), prevented platelet activation and secretion by inhibiting rho-associated kinase (ROCK) activity *in vitro* (Kardeby et al., 2019). However, ROCK activation was not affected in AoSMCs (data not shown), which is supported by previous studies where the commercial ROCK inhibitor Y-27632, had minimal effects on LPS induced IL-1β responses in AoSMCs Wei et al., 2006). Therefore, it is unlikely that MK118 or MK196 inhibits ROCK in AoSMCs and thereby affects the IL-1β levels.

The *in silico* studies attempted to explore the binding profile of the purine analogues MK118 and MK196, at JAK1-3 active site. The derived MD results indicated that the purine-piperazine scaffold is well accommodated in the ATP binding cleft of the three JAK isoforms, while the purine moiety engages crucial residues of the hinge region through the whole simulation time.

The terminal nitrate ester of MK118 consists a promising pharmacophore able to contact critical residues in the active site of JAK1-3. Specifically, the binding orientation of MK118 resembles that of CP-6909550 (Tofacitinib) orienting its nitro ester group towards the Gly loop. Thus, the inhibitory activity of MK118 against the kinase isoforms may correlate with the ionic interactions of this group with conserved residues of the DFG motif (Asp1021 in JAK1 and Asp994 in JAK2) and the catalytic residues in the neighboring of Gly loop (Lys908 in JAK1 and Lys882 in JAK2) or even residues of the Gly loop (Lys830 at JAK3). Future optimization should include some degree of rigidification in order to increase the stability of the developed interactions of the nitro group.

The absence of the terminal nitro moiety is associated with an increased flexibility of the alkyl chain, as shown by the derived binding motifs of MK196 in the active site of all JAK isoforms. However, MK196 uses its carbonyl moiety to enable direct and indirect H-bond interactions with Gly loop (Glu883 at JAK1 and Lys857 in JAK2) and the DFG motif (Asp1021 at JAK1), which may contribute positively to its binding affinity and inhibitory activity. It is worth mentioning that in the case of JAK3, MK196 establishes direct contact with the unique Cys909 and a water mediated interaction with the conserved Arg953 located in the catalytic loop. The contact with Cys909 could drive our optimization strategy towards JAK3 specific inhibitors.

An additional aim of the present study was to explore the ability of MK118 and MK196 to regulate other inflammatory proteins. Olink

proteomics showed that MK118 and MK196 regulate the release of several additional proteins involved in inflammation and CVD, including TRAIL, CCL4, CSF1 and CCL3. TRAIL was downregulated by MK118 and MK196 and previous studies have shown that TRAIL receptors are expressed by vascular smooth muscle cells and cardiomyocytes, but only at low levels in endothelial cells (Cheng et al., 2014). However, the role of TRAIL in atherosclerosis and inflammation is debated. Deletion of TRAIL has been shown to increase the lesion size in ApoE$^{-/-}$ mice (Watt et al., 2011). In contrast, *in vitro* studies have shown that TRAIL can promote inflammation via NF-κB in vascular smooth muscle cells, and NF-κB is known to induce several proinflammatory biomarkers (Cheng et al., 2014; Kavurma et al., 2008). Furthermore, we found that the chemokines CCL3 and CCL4, also known as MIP-1α and MIP-1β/M-CSF respectively, were downregulated by MK118 and MK196. Previous studies have shown that inhibition of CCL3 or CCL4 resulted in reduced atherosclerotic areas and more stable lesions in LDLR$^{-/-}$ or ApoE$^{-/-}$ mice respectively (Kennedy et al., 2012; Chang et al., 2020). Moreover, CSF1 was also found downregulated by MK118 and MK196. CSF1 is a cytokine highly expressed in atherosclerotic lesions (Rosenfeld et al., 1992). CSF1 is proatherogenic and atherosclerotic mouse models lacking CSF1 show reduced atherosclerosis (reviewed in Mindur and Swirski, 2019). We also observed that cytokines and chemokines, such as IL-7, CXCL10, PD-L1, FLT3L and CCL20 were significantly downregulated by MK196 but not by MK118. The precise mechanism underlying MK196-specific effect on inflammation biomarkers is currently unknown and can reasonably not be explained by only a drug-interaction with JAK 1–3. The differences in protein regulations between MK118 and MK196 is however beyond the focus of the present study and additional studies are warranted to elucidate the role of purine analogues as modulators of inflammation in CVD.

5. Conclusion

Collectively, the present study attempted to shed light at the anti-inflammatory effect of the two purine analogues MK118 and MK196 and further investigate the importance of the nitrate-ester moiety on the side chain of MK118. We conclude that MK118 and MK196 inhibit the LPS-induced release of inflammatory proteins such as TRAIL, CCL4, CSF1 and IL-1β in AoSMCs and it is noteworthy that the Olink proteomics analysis revealed that the absence of the nitro group in MK196 was associated with broader effects on inflammation biomarker profile. We showed that the nitrate-ester moiety in MK118 participates in binding interactions with crucial amino acids of the molecular targets JAK 1–3 and that this may be associated with a trend to more efficiently inhibition of JAKs in biological assays. MK118 also significantly regulate the expression of several NLRP3 inflammasome components at both transcriptional and protein levels in AoSMCs. A similar trend was observed for MK196. These findings serve as the foundation for subsequent studies to yield additional insight on the anti-inflammatory role of MK118 and MK196, as well as on the design and structural optimization of novel purine analogues.

CRediT authorship contribution statement

Geena V. Paramel: Conceptualization, Methodology, Investigation, Formal analysis, Visualization, Supervision, Writing – review & editing. **Madelene Lindkvist:** Investigation, Methodology, Formal analysis, Visualizsation, Writing – review & editing. **Berhane A. Idosa:** Investigation, Formal analysis, Methodology. **Laila Sharon Sebina:** Investigation, Formal analysis, Methodology. **Caroline Kardeby:** Formal analysis, Writing – review & editing. **Theano Fotopoulou:** Investigation, Formal analysis. **Dimitra Pournara:** Investigation, Formal analysis. **Eftichia Kritsi:** Investigation, Formal analysis. **Eleni Ifanti:** Investigation, Formal analysis. **Maria Zervou:** Resources, Supervision, Writing – review & editing. **Maria Koufaki:** Conceptualization, Resources, Funding acquisition, Supervision, Writing – review & editing. **Magnus Grenegård:** Conceptualization, Supervision, Writing – review & editing. **Karin Fransén:** Conceptualization, Resources, Supervision, Writing – original draft, Writing – review & editing, Funding acquisition.

Declaration of interests

The authors declare that they have no known competing financial interests or personal relationships that could have appeared to influence the work reported in this paper.

Acknowledgements

This work was supported by grants from The Knowledge Foundation HÖG2017 #20170191 (PI Karin Fransén); The Knowledge Foundation HÖG2019 #20190088 (PI Karin Fransén); Örebro University, Faculty of Medicine and Health #2019-06-13 (PI Karin Fransén). Dimitra Pournara was supported by Alexander S Onassis Public Benefit Foundation fellowship, PI Maria Koufaki.

Appendix A. Supplementary data

Supplementary data to this article can be found online at https://doi.org/10.1016/j.ejphar.2022.175128.

References

Assarsson, E., Lundberg, M., Homlquist, G., Björkesten, G., Bucht Thorsen, S., Ekman, D., Eriksson, A., Rellen Dickens, E., Ohlsson, S., Edfeldt, G., Andersson, A.-C., Lindstedt, P., Stenvang, J., Gullberg, M., Fredriksson, S., 2014. Homogenous 96-plex PEA immunoassay exhibiting high sensitivity, specificity, and excellent scalability. PLoS One 9, e95192.

Bauernfeind, F., Ablasser, A., Bartok, E., Kim, S., Schmid-Burgk, J., Cavlar, T., Hornung, V., 2011. Inflammasomes: current understanding and open questions. Cell. Mol. Life Sci. 68, 765–783.

Chang, T.T., Yang, H.Y., Chen, C., Chen, J.W., 2020. CCL4 inhibition in atherosclerosis: effects on plaque stability, endothelial cell adhesiveness, and macrophages activation. Int. J. Mol. Sci. 21, 6567.

Cheng, W., Zhao, Y., Wang, S., Jiang, F., 2014. Tumor necrosis factor-related apoptosis-inducing ligand in vascular inflammation and atherosclerosis: a protector or culprit? Vasc. Pharmacol. 63, 135–144.

Cornut, M., Bourdonnay, E., Henry, T., 2020. Transcriptional regulation of inflammasomes. Int. J. Mol. Sci. 21, 8087.

Dautova, Y., Kapustin, A.N., Pappert, K., Epple, M., Okkenhaug, H., Cook, S.J., Shanahan, C.M., Bootman, M.D., Proudfoot, D., 2018. Calcium phosphate particles stimulate interleukin-1β release from human vascular smooth muscle cells: a role for spleen tyrosine kinase and exosome release. J. Mol. Cell. Cardiol. 115, 82–93.

Fu, X.Q., Liu, B., Wang, Y.P., Li, J.K., Zhu, P.L., Li, T., Tse, K.W., Chou, J.Y., Yin, C.L., Bai, J.X., Liu, Y.X., Chen, Y.J., Yu, Z.L., 2020. Activation of STAT3 is a key event in TLR4 signaling-mediated melanoma progression. Cell Death Dis. 11, 246.

Furuya, M.Y., Asano, T., Sumichika, Y., Sato, S., Kobayashi, H., Watanabe, H., Suzuki, E., Kozuru, H., Yatsuhashi, H., Koga, T., Ohira, H., Sekine, H., Kawakami, A., Migita, K., 2018. Tofacitinib inhibits granulocyte-macrophage colony-stimulating factor-induced NLRP3 inflammasome activation in human neutrophils. Arthritis Res. Ther. 20, 196.

Hansson, G.K., 2009. Atherosclerosis–an immune disease: the anitschkov lecture 2007. Atherosclerosis 202, 2–10.

Kardeby, C., Paramel, G.V., Pournara, D., Fotopoulou, T., Sirsjö, A., Koufaki, M., Fransén, K., Grenegård, M., 2019. A novel purine analogue bearing nitrate ester prevents platelet activation by ROCK activity inhibition. Eur. J. Pharmacol. 857, 172428.

Kavurma, M.M., Schoppet, M., Bobryshev, Y.V., Khachigian, L.M., Bennett, M.R., 2008. TRAIL stimulates proliferation of vascular smooth muscle cells via activation of NF-kappaB and induction of insulin-like growth factor-1 receptor. J. Biol. Chem. 283, 7754–7762.

Kennedy, A., Gruen, M.L., Gutierrez, D.A., Surmi, B.K., Orr, J.S., Webb, C.D., Hasty, A.H., 2012. Impact of macrophage inflammatory protein-1α deficiency on atherosclerotic lesion formation, hepatic steatosis, and adipose tissue expansion. PLoS One 7, e31508.

Koufaki, M., Fotopoulou, T., Iliodromitis, E.K., Bibli, S.E., Zoga, A., Kremastinos, D.K., Andreadou, I., 2012. Discovery of 6-[4-(6-nitroxyhexanoyl)piperazin-1-yl)]-9H-purine, as pharmacological post-conditioning agent. Bioorg. Med. Chem. 20, 5948–5956.

Lai, S.Y., Johnson, F.M., 2010. Defining the role of the JAK-STAT pathway in head and neck and thoracic malignancies: implications for future therapeutic approaches. Drug Resist. Updates 13, 67–78.

Lee, C., Lim, H.K., Sakong, J., Lee, Y.S., Kim, J.R., Baek, S.H., 2006. Janus. kinase-signal transducer and activator of transcription mediates phosphatidic acid-induced interleukin (IL)-1beta and IL-6 production. Mol. Pharmacol. 69, 1041–1047.
Libby, P., 2017. Interleukin-1 beta as a target for atherosclerosis therapy: the biological basis of CANTOS and beyond. J. Am. Coll. Cardiol. 70, 2278–2289.
Lin, T.E., HuangFu, W.C., Chao, M.W., Sung, T.Y., Chang, C.D., Chen, Y.Y., Hsieh, J.H., Tu, H.J., Huang, H.L., Pan, S.L., Hsu, K.C., 2018. A novel selective JAK2 inhibitor identified using pharmacological interactions. Front. Pharmacol. 9, 1379.
Lundberg, M., Eriksson, A., Tran, B., Assarsson, E., Fredriksson, S., 2011. Homogeneous antibody-based proximity extension assays provide sensitive and specific detection of low-abundant proteins in human blood. Nucleic Acids Res. 39, e102.
Martinon, F., Tschopp, J., 2005. NLRs join TLRs as innate sensors of pathogens. Trends Immunol. 26, 447–454.
Maugé, L., Fotopoulou, T., Delemasure, S., Dutartre, P., Koufaki, M., Connat, J.L., 2014. In vitro inflammatory/anti-inflammatory effects of nitrate esters of purines. Eur. J. Pharmacol. 730, 148–156.
Mindur, J.E., Swirski, F.K., 2019. Growth factors as immunotherapeutic targets in cardiovascular disease. Arterioscler. Thromb. Vasc. Biol. 39, 1275–1287.
Moyer, C.F., Sajuthi, D., Tulli, H., Williams, J.K., 1991. Synthesis of IL-1 alpha and IL-1 beta by arterial cells in atherosclerosis. Am. J. Pathol. 138, 951–960.
Paramel Varghese, G., Folkersen, L., Strawbridge, R.J., Halvorsen, B., Yndestad, A., Ranheim, T., Krohg-Sørensen, K., Skjelland, M., Espevik, T., Aukrust, P., Lengquist, M., Hedin, U., Jansson, J.H., Fransén, K., Hansson, G.K., Eriksson, P., Sirsjö, A., 2016. NLRP3 inflammasome expression and activation in human atherosclerosis. J. Am. Heart Assoc. 5, e003031.
Pellegrini, C., Antonioli, L., Lopez-Castejon, G., Blandizzi, C., Fornai, M., 2017. Canonical and non-canonical activation of NLRP3 inflammasome at the crossroad between immune tolerance and intestinal inflammation. Front. Immunol. 8, 36.
Ramji, D.P., Davies, T.S., 2015. Cytokines in atherosclerosis: key players in all stages of disease and promising therapeutic targets. Cytokine Growth Factor Rev. 26, 673–685.
Ridker, P.M., Everett, B.M., Thuren, T., MacFadyen, J.G., Chang, W.H., Ballantyne, C., Fonseca, F., Nicolau, J., Koenig, W., Anker, S.D., Kastelein, J.J.P., Cornel, J.H., Pais, P., Pella, D., Genest, J., Cifkova, R., Lorenzatti, A., Forster, T., Kobalava, Z., Vida-Simiti, L., Flather, M., Shimokawa, H., Ogawa, H., Dellborg, M., Rossi, P.R.F., Troquay, R.P.T., Libby, P., Glynn, R.J., CANTOS Trial Group, 2017. Antiinflammatory therapy with canakinumab for atherosclerotic disease. N. Engl. J. Med. 377, 1119–1131.
Rosenfeld, M.E., Ylä-Herttuala, S., Lipton, B.A., Ord, V.A., Witztum, J.L., Steinberg, D., 1992. Macrophage colony-stimulating factor mRNA and protein in atherosclerotic lesions of rabbits and humans. Am. J. Pathol. 140, 291–300.
Samavati, L., Rastogi, R., Du, W., Hüttemann, M., Fite, A., Franchi, L., 2009. STAT3 tyrosine phosphorylation is critical for interleukin 1 beta and interleukin-6 production in response to lipopolysaccharide and live bacteria. Mol. Immunol. 46, 1867–1877.
Schrödinger Release 2020-3, 2020. LigPrep, Schrödinger, LLC, New York, NY.
Schrödinger Release 2020-3, 2020. Glide, Schrödinger, LLC, New York, NY.
Schrödinger Release 2020-3, 2020c. Protein Preparation Wizard. Epik, Schrödinger, LLC, New York, NY, 2021; Impact, Schrödinger, LLC, New York, NY; Prime, Schrödinger, LLC, New York, NY.
Schrödinger Release 2020-3, 2020d. Desmond Molecular Dynamics System. D. E. Shaw Research, New York, NY, 2020. Maestro-Desmond Interoperability Tools, Schrödinger, New York, NY.
Schuringa, J.J., Wierenga, A.T., Kruijer, W., Vellenga, E., 2000. Constitutive Stat3, Tyr705, and Ser727 phosphorylation in acute myeloid leukemia cells caused by the autocrine secretion of interleukin-6. Blood 95, 3765–3770.
Sodhi, A., Tarang, S., Kesherwani, V., 2007. Concanavalin A induced expression of Toll-like receptors in murine peritoneal macrophages in vitro. Int. Immunopharm. 7, 454–463.
Thorarensen, A., Dowty, M.E., Banker, M.E., Juba, B., Jussif, J., Lin, T., Vincent, F., Czerwinski, R.M., Casimiro-Garcia, A., Unwalla, R., Trujillo, J.I., Liang, S., Balbo, P., Che, Y., Gilbert, A.M., Brown, M.F., Hayward, M., Montgomery, J., Leung, L., Yang, X., Soucy, S., Hegen, M., Coe, J., Langille, J., Vajdos, F., Chrencik, J., Telliez, J. B., 2017. Design of a janus kinase 3 (JAK3) specific inhibitor 1-((2S,5R)-5-((7H-Pyrrolo[2,3-d]pyrimidin-4-yl)amino)-2-methylpiperidin-1-yl)prop-2-en-1-one (PF-06651600) allowing for the interrogation of JAK3 signaling in humans. J. Med. Chem. 60, 1971–1993.
Vazquez, M.L., Kaila, N., Strohbach, J.W., Trzupek, J.D., Brown, M.F., Flanagan, M.E., Mitton-Fry, M.J., Johnson, T.A., TenBrink, R.E., Arnold, E.P., Basak, A., Heasley, S. E., Kwon, S., Langille, J., Parikh, M.D., Griffin, S.H., Casavant, J.M., Duclos, B.A., Fenwick, A.E., Harris, T.M., Han, S., Caspers, N., Dowty, M.E., Yang, X., Banker, M. E., Hegen, M., Symanowicz, P.T., Li, L., Wang, L., Lin, T.H., Jussif, J., Clark, J.D., Telliez, J.B., Robinson, R.P., Unwalla, R., 2018. Identification of N-{cis-3-[Methyl (7H-pyrrolo[2,3-d]pyrimidin-4-yl)amino]cyclobutyl}propane-1-sulfonamide (PF-04965842): a selective JAK1 clinical candidate for the treatment of autoimmune diseases. J. Med. Chem. 61, 1130–1152.
Villarino, A.V., Kanno, Y., Ferdinand, J.R., O'Shea, J.J., 2015. Mechanisms of Jak/STAT signaling in immunity and disease. J. Immunol. 194, 21–27.
Watt, V., Chamberlain, J., Steiner, T., Francis, S., Crossman, D., 2011. TRAIL attenuates the development of atherosclerosis in apolipoprotein E deficient mice. Atherosclerosis 215, 348–354.
Wei, C.Y., Huang, K.C., Chou, Y.H., Hsieh, P.F., Lin, K.H., Lin, W.W., 2006. The role of Rho-associated kinase in differential regulation by statins of interleukin-1beta- and lipopolysaccharide-mediated nuclear factor kappaB activation and inducible nitric-oxide synthase gene expression in vascular smooth muscle cells. Mol. Pharmacol. 69, 960–967.
Williams, N.K., Bamert, R.S., Patel, O., Wang, C., Walden, P.M., Wilks, A.F., Fantino, E., Rossjohn, J., Lucet, I.S., 2009. Dissecting specificity in the Janus kinases: the structures of JAK-specific inhibitors complexed to the JAK1 and JAK2 protein tyrosine kinase domains. J. Mol. Biol. 387, 219–232.